In vitro system using human neurons demonstrates that varicella-zoster vaccine virus is impaired for reactivation, but not latency

Tomohiko Sadaoka[a,1], Daniel P. Depledge[b], Labchan Rajbhandari[c], Arun Venkatesan[c], Judith Breuer[b], and Jeffrey I. Cohen[a,2]

[a]Medical Virology Section, Laboratory of Infectious Diseases, National Institute of Allergy and Infectious Diseases, National Institutes of Health, Bethesda, MD 20892; [b]Division of Infection and Immunity, MRC Centre for Medical Molecular Virology, University College London, London WC1E 6BT, United Kingdom; and [c]Division of Neuroimmunology and Neuroinfectious Diseases, Department of Neurology, Johns Hopkins University School of Medicine, Johns Hopkins Hospital, Baltimore, MD 21287

Edited by Diane E. Griffin, Johns Hopkins Bloomberg School of Public Health, Baltimore, MD, and approved March 18, 2016 (received for review November 15, 2015)

Varicella-zoster virus (VZV) establishes latency in human sensory and cranial nerve ganglia during primary infection (varicella), and the virus can reactivate and cause zoster after primary infection. The mechanism of how the virus establishes and maintains latency and how it reactivates is poorly understood, largely due to the lack of robust models. We found that axonal infection of neurons derived from hESCs in a microfluidic device with cell-free parental Oka (POka) VZV resulted in latent infection with inability to detect several viral mRNAs by reverse transcriptase-quantitative PCR, no production of infectious virus, and maintenance of the viral DNA genome in endless configuration, consistent with an episome configuration. With deep sequencing, however, multiple viral mRNAs were detected. Treatment of the latently infected neurons with Ab to NGF resulted in production of infectious virus in about 25% of the latently infected cultures. Axonal infection of neurons with vaccine Oka (VOka) VZV resulted in a latent infection similar to infection with POka; however, in contrast to POka, VOka-infected neurons were markedly impaired for reactivation after treatment with Ab to NGF. In addition, viral transcription was markedly reduced in neurons latently infected with VOka compared with POka. Our in vitro system recapitulates both VZV latency and reactivation in vivo and may be used to study viral vaccines for their ability to establish latency and reactivate.

varicella-zoster virus | varicella vaccine | reactivation | latency | herpesvirus

Varicella-zoster virus (VZV) is a member of Alphaherpesvirinae, characterized by neurotropism and lifelong latent infection in human dorsal root, cranial nerve, and enteric ganglia (1). During primary infection (varicella), VZV gains access to sensory neurons by two potential routes: retrograde axonal transport from cutaneous lesions or infection of neurons by virus-infected T cells circulating through the body (2). The virus then establishes latency in neurons, and months to years later, when VZV-specific T cells decline, the virus can reactivate to cause herpes zoster.

VZV is the only human herpesvirus for which a licensed vaccine is approved, and the live-attenuated vaccine Oka (VOka) virus is effective in preventing both varicella and zoster. VOka was derived from WT parental Oka (POka) by propagation in human embryonic lung cells, guinea pig embryo fibroblasts, and human fibroblasts (3, 4). VOka is a genetic mixture of at least eight genotypes (5), and, initially, the genomes of POka and VOka were found to differ by 42 nucleotides and 20 amino acids (6). A recent study using deep sequencing identified 165 additional nucleotide changes in VOka, although most changes were presence in <10% of viral genomes (7). Attenuation of VOka is postulated to be due to mutations in multiple regions of the genome (8, 9).

Despite numerous studies, the mechanisms for establishment and maintenance of VZV latency and subsequent reactivation remain poorly understood, primarily due to the lack of robust in vivo and in vitro models for latency. Several rodent models for VZV latency have been explored to date, but none has demonstrated reactivation (10). Although simian varicella virus can establish latency and reactivation in monkeys, there are important differences in the simian and human varicella viral genomes, and these experiments are limited by the cost associated with these animals (11). Human cadaveric ganglia have been used to study viral transcripts and proteins expressed during latency. Although several VZV mRNAs and proteins have been detected in human ganglia (12), more recent studies suggest that viral protein expression during latency observed in certain prior studies may be due to nonspecific Ab staining (13, 14), and viral mRNA expression has been postulated to reflect postmortem events rather than the true latent state (15). Recent advances in stem cell research allow a virtually unlimited supply of human neurons differentiated from hESCs or human-induced pluripotent stem cells that have not been infected with VZV. The use of stem cell-derived neurons contrasts with the use of neurons from sensory or cranial nerve ganglia isolated from human cadavers, most of which have already been infected with VZV. Neurons from hESCs fully support lytic infection after infection with cell-associated POka VZV of either the cell body (soma) or axons through retrograde transport using compartmented microfluidic chambers (16, 17). In this model, the cellular transcriptome in

Significance

The varicella vaccine is highly effective in preventing chickenpox. Although the vaccine virus is attenuated, it is unknown whether the virus is impaired for establishment of latency, for reactivation, or both. We developed an in vitro system using human neurons derived from ES cells and showed that axonal infection of neurons results in latent infection and that virus can be reactivated using Ab to NGF. Using this system, we show that the varicella vaccine is impaired for reactivation, but not latency. Although not necessarily equivalent to varicella-zoster virus (VZV) latency and reactivation in vivo, this system may be used to study the ability of other viruses, including viral vaccines, to establish latency and reactivate.

Author contributions: T.S., A.V., J.B., and J.I.C. designed research; T.S., D.P.D., and L.R. performed research; T.S., D.P.D., L.R., A.V., J.B., and J.I.C. analyzed data; and T.S., D.P.D., A.V., J.B., and J.I.C. wrote the paper.

The authors declare no conflict of interest.

This article is a PNAS Direct Submission.

[1]Present address: Division of Clinical Virology, Center for Infectious Diseases, Kobe University Graduate School of Medicine, 7-5-1 Kusunoki-cho, Chuo-ku, Kobe 650-0017, Japan.

[2]To whom correspondence should be addressed. Email: jcohen@niaid.nih.gov.

This article contains supporting information online at www.pnas.org/lookup/suppl/doi:10.1073/pnas.1522575113/-/DCSupplemental.

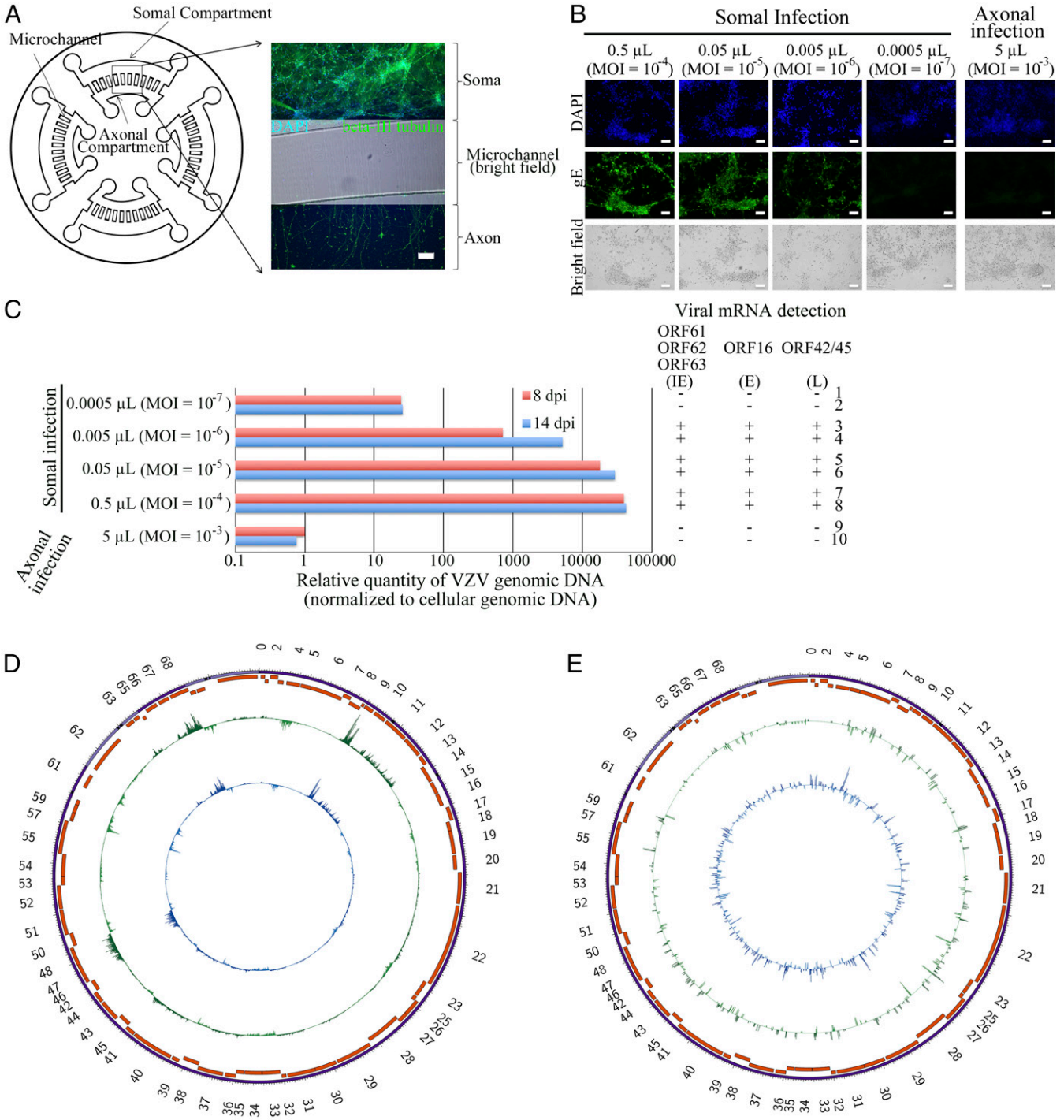

Fig. 1. Somal infection of human neurons with VZV usually induces productive infection, but axonal infection results in persistent infection. (*A*) hESC (H9)-derived NSCs were seeded in the somal compartment (1×10^5 cells per sector) of a microfluidic device and differentiated into neurons for 21–30 d until abundant neurite outgrowth was observed in the axonal compartment. Neurons were stained with anti-beta III tubulin Ab and DAPI. (Scale bar, 100 μm.) (*B* and *C*) Neurons were infected with WT POka VZV cell-free virus at the indicated MOI in the somal or axonal compartment of the microfluidic device. (*B*) At 8 dpi, cells were stained with VZV anti-gE Ab and DAPI. (Scale bars, 50 μm.) (*C*) At 8 and 14 dpi, DNA and RNA were extracted from the infected cells, cDNA was synthesized from RNA, and RT-qPCR was performed. (*Left*) Relative quantity of VZV DNA (using VZV ORF61 primers) to cellular genomic DNA (using CD24 gene primers) is shown based on axonal infection at 8 dpi. (*Right*) VZV mRNAs from different kinetic classes were analyzed: ORF62 and ORF63, immediate-early (IE) and ORF61 putative IE genes; ORF16, a putative early gene (E); and ORF42/45, a putative late gene (L). +, detected; –, not detected. Circos plot shows VZV POka (*D*) and VOka (*E*) mRNA expression in neurons 14 d after selective axonal infection. The outer track shows the VZV genome in its prototypic orientation. The blue and green tracks show the mean read depth in nonoverlapping 25-bp windows for the stranded RNA-seq library from two independent experiments (blue track performed in duplicate and green track performed in triplicate) and are analogous to gene expression. The peaks facing outward from the center indicate genes expressed on the positive strand, whereas the peaks facing inward indicate genes expressed on the negative strand. The *y* axis for the peaks are the number of reads from mRNA-seq scaled from 0 to 15,000 for POka and from 0 to 15 for VOka.

productively infected neurons is different from the cellular transcriptome reported for fibroblasts, T cells, and keratinocytes (18–20). Recently, Markus et al. (21) reported an in vitro model of latency and reactivation of VZV in hESC-derived neurons using a compartmented microfluidic chamber and selective axonal infection of POka-based recombinant virus. A latent infection could be established with expression of multiple VZV mRNAs at low levels; induction of reactivation by a phosphoinositide 3-kinase (PI3K) inhibitor resulted in spreading of VZV ORF66 protein kinase-fused GFP within a cluster of neurons.

Here, we report an in vitro system using selective axonal infection of human neurons derived from hESCs that allows establishment and maintenance of latent VZV in which virus reactivation can be induced with Ab to NGF. We use this system to show that although VOka can establish latency with a similar efficiency as POka, VOka is impaired for reactivation.

Methods

Cells and Viruses. hESC (H9)-derived neural stem cells (NSCs) were cultured in StemPro NSC SFM complete medium (Life Technologies) consisting of KnockOut DMEM/F-12 (Life Technologies) with StemPro Neural Supplement [2% (vol/vol); Life Technologies], EGF (20 ng/mL), basic FGF (20 ng/mL), and GlutaMAX-I (2 mM; Life Technologies) as adherent cells in flasks or plates coated with CELLStart (1:100) according to the manufacturer's instructions (Life Technologies). The use of commercially sourced NSCs is excluded from NIH Institutional Review Board review and Office of Human Subjects Research Protections determination consistent with the NIH Human Research Protection Program. NSCs were used after the second to 10th passages. Neurons were differentiated from H9-derived NSCs in neural differentiation medium consisting of neurobasal medium with B-27 serum-free supplement [2% (vol/vol)] and GlutaMAX-I (2 mM) for least 11 d in 12-well plates or a microfluidic device coated with CELLStart (1:100) or poly-D-lysine (PDL; 200 μg/mL; Sigma–Aldrich) and Matrigel (1.25 μg/mL; Corning). Human lung (MRC-5) fibroblasts were cultured in minimum essential medium (MEM; Life Technologies) supplemented with 10% (vol/vol) heat-inactivated FBS (Sigma–Aldrich) and GlutaMAX-I (2 mM).

The VZV POka was kindly provided by Michiaki Takahashi (Osaka University, Suita, Osaka, Japan), and VOka (Zostavax) was purchased from Merck. Viruses were propagated on MRC-5 cells, and cell-free virus was prepared as previously described (22); cells were disrupted using a Misonix sonicator 3000.

Cell-free VZV was titrated by serial 10-fold dilutions in 400 μL of culture medium and added to MRC-5 cells for 1 h at 37 °C, washed twice with MEM, and cultured for 7 d. Cells were fixed with 4% (vol/vol) paraformaldehyde in PBS and stained with mouse monoclonal anti-VZV glycoprotein E (gE) Ab (1:3,000, clone 8612; EMD Millipore), followed by ECL anti-mouse IgG HRP-linked whole Ab (1:3,000; GE Healthcare Bio-Sciences). Plaques were visualized with 3, 3′, 5, 5′-tetramethylbenzidine-H peroxidase substrate (Moss, Inc.) and counted.

Microfluidic Devices and Neuron Cultures. A four-well polydimethylsiloxane-based microfluidic device comprised of two compartments (length = 8 mm, width = 1 mm) separated by an array of 200 microchannels (length = 500 μm, width = 10 μm, height = 2.5 μm) (Fig. 1) was fabricated as previously described (23). We previously showed that these devices allow selective growth of axons in one compartment, enable isolation of cell soma from their axons, and allow independent manipulation of somal and axonal compartments (24–26). To allow cells to adhere to the device, the devices were treated with PDL and Matrigel. A 200-μg/mL solution of PDL diluted in molecular-grade water was introduced by way of access ports and incubated overnight at 37 °C in a humidified 5% CO_2 incubator, and the device was washed three times with double-deionized water to remove unbound PDL. The device was then coated with a 1.25-μg/mL solution of Matrigel diluted in KnockOut DMEM/F-12 and incubated for 2 h at room temperature, followed by overnight incubation at 37 °C in a humidified 5% CO_2 incubator, and maintained at room temperature until use.

For differentiation of NSCs into neurons, 4 μL of NSCs (2.5×10^7 cells per milliliter) was loaded into the somal compartment of the device in neural differentiation medium, and 20 μL of medium was added in the axonal compartment to prevent movement of NSCs from the somal compartment to the axonal compartment. The cells were cultured for 2 h at 37 °C in a humidified 5% CO_2 incubator, and medium was added to each compartment with a higher medium level in the axonal compartment to prevent the movement of NSCs from the somal compartment to the axonal compartment. Half of the medium was changed every 4 d, and cells were maintained until axons were observed in the axonal compartment (typically 21–30 d post-differentiation). Differentiation into neurons was confirmed by neurite outgrowth and expression of beta-III tubulin as a neuron-specific marker. Neurons were fixed with 4% paraformaldehyde in PBS, permeabilized with 0.1% Triton X-100, and stained with mouse monoclonal anti–beta-III tubulin Ab (1:100, clone SDL.3D10; Sigma-Aldrich) followed by Alexa Fluor 488-labeled donkey anti-mouse IgG Ab (1:200; Life Technologies) and DAPI (Invitrogen).

Immunofluorescence Studies of Neuron Cultures. Neuron cultures were washed with PBS, fixed for 20 min with 4% (vol/vol) paraformaldehyde, washed again, and incubated in blocking solution (0.25% Triton X-100 and 5% normal donkey serum) for 1 h. Cells were stained with the following primary Abs diluted in blocking solution overnight: mouse anti–β-III-tubulin (a marker for neurons; 1:1,000; Abcam); rabbit anti–microtubule-associated protein (Map2), a marker for neurons (1:200; Sigma); mouse anti-Brn3a, a marker for sensory neurons (1:200; Chemicon); rabbit and goat antiperipherin, a marker for peripheral nervous system neurons (1:200; Abcam and 1:200; Santa Cruz Biotechnology, respectively); rabbit anti-GFAP, a marker of cells of astrocyte origin (1:1,000; Dako); rabbit anti–IBA-1, a marker for microglia (1:500; Wako Chemicals); rabbit anti-Olig2, a marker for oligodendrocytes (1:200; Millipore); and mouse anti-myelin basic protein (MBP), a marker of oligodendrocytes (1:1,000; Covance). Cells were then washed, incubated with Alexa Fluor-conjugated donkey secondary Abs for 2 h, washed, incubated for 5 min with 1 μM of DAPI as a nuclear counterstain, and imaged.

Virus Infections. Neurons were infected with VZV at the somal (cell body) or axonal compartment for 2 h at 37 °C using a multiplicity of infection (MOI) based on the titer of virus obtained in MRC-5 cells. After 2 h, the virus inoculum was removed, cells were washed with medium and treated with low pH buffer [40 mM sodium citrate, 10 mM potassium chloride, 135 mM sodium chloride (pH 3.2)] for 30 s to inactivate virus that had not entered the cells as described previously (27), and neural differentiation medium was added. For virus reactivation, anti-NGF Ab (AB1528SP; EMD Millipore) was added to the somal and axonal compartments at a final concentration of 50 μg/mL and cultured for 7 d. IgG isotype control Ab (Purified Sheep IgG; R&D Systems) was used as a negative control. Cells were fixed with 4% (vol/vol) paraformaldehyde in PBS, permeabilized with 0.1% Triton X-100, and stained with mouse monoclonal anti-VZV gE Ab (1:500, clone 8612) followed by Alexa Fluor 488-labeled donkey anti-mouse IgG Ab (1:200) and DAPI.

DNA and RNA Isolation, cDNA Synthesis, and Quantitative PCR. Total DNA and RNA were isolated from cells using an AllPrep DNA/RNA Mini Kit (Qiagen) according to the manufacturer's instructions. DNA was eluted from the column in 100 μL of elution buffer, and RNA was treated with recombinant DNase I (5 units per 100 μL; Roche Diagnostics) for 1 h at 37 °C and then eluted in 30 μL of nuclease-free water. The cDNA was synthesized with 10.4 μL of RNA and anchored-oligo$(dT)_{18}$ primer in a 20-μL reaction using a Transcriptor High Fidelity cDNA synthesis kit (Roche Diagnostics).

Relative quantitative PCR (qPCR) and absolute qPCR were performed using DNA and RNA extracted from 5×10^4 cells per reaction. One microliter of DNA (representing 1% of the total DNA extracted) or 1 μL of cDNA (obtained from 3.3% of the total RNA extracted) was used in a 15-μL reaction in duplicate with FastStart Universal SYBR Green Master (Rox; Roche Diagnostics) in a 7500 Real-Time PCR System (Life Technologies). The qPCR program was 1 cycle of 95 °C hot start for 10 min and 45 cycles of 95 °C for 15 s and 60 °C for 45 s. For relative qPCR, primers for CD24 were used as a DNA internal control and primers for beta-actin to amplify cDNA were used as an RNA internal control. VZV genomic DNA was quantified by amplification of ORF61 for relative qPCR. For absolute qPCR, a standard curve was generated using 10-fold serial dilutions of known copy number (10^6 to 1) of VZV POka BAC genome (VZV_{Luc} BAC was a kind gift from Hua Zhu, New Jersey Medical School, Rutgers University, Newark, NJ) (28). A dissociation curve analysis from 60 to 95 °C was performed after every qPCR run to exclude primer-dimer formation and other nonspecific amplification. Viral mRNA was detected by amplification of cDNAs from immediate-early genes ORF62 and ORF63, a putative immediate-early gene ORF61, a putative early gene ORF16, and putative late gene ORF42/45. Primer sequences are listed in Table S1.

VZV DNA Configuration. VZV DNA configuration was determined by the ratio of genomes with fused termini to linear genomes (29) with slight modifications. The copy number of fused termini was determined by qPCR using primers T1 and T2, and the copy number of linear genomes was quantified using primers to ORF49 (ORF49F21 and R80; Fig. 2*A*). A standard curve for circular genomes was generated using VZV_{Luc} BAC. The qPCR conditions

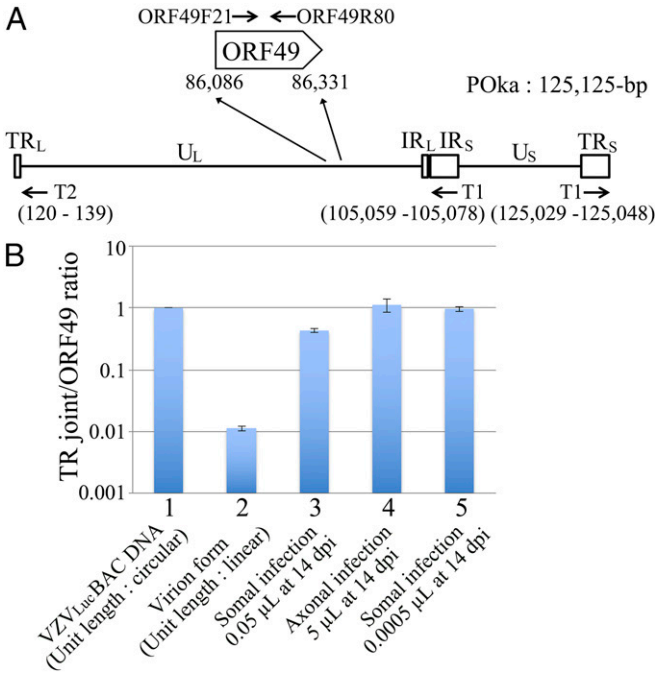

Fig. 2. The VZV genome is maintained in axonal infected neurons with fused VZV genomic termini, suggesting a circular or episomal configuration. (*A*) Map of the POka strain VZV genome and primers (T1, T2) used to detect fused genomic termini and primers (ORF49F21, ORF49R80) used to detect the internal region of the genome. The genome contains unique long (U_L), unique short (U_S), internal repeat (IR), and terminal repeat (TR) regions. (*B*) Neurons were infected with POka VZV cell-free virus with the indicated amount of virus aliquot (with MOI based on the virus titer measured in MRC-5 cells) in the somal or axonal compartment of the microfluidic device. At indicated time points, DNA was extracted from the cells and qPCR was performed. Full-length VZV_{Luc} BAC, in which the viral genomic termini are fused, was used as a control for episomal (circular) viral DNA, and VZV cell-free virus DNA was used as a control for linear viral DNA without fused termini. The ratio of the absolute copy number of PCR products using VZV termini primers to VZV internal primers was calculated. Absolute copy number was determined based on standard curves derived from 1 to 10^6 copies of unit-length circular VZV-BAC DNA. The amplification efficiency of the qPCR reaction was calculated based on the slope of the standard curves and was 1.88–2.11 for ORF49 and 1.28–1.33 for TR joint.

were one cycle of 95 °C hot start for 10 min and 45 cycles of 95 °C for 15 s, 58 °C for 10 s, and 72 °C for 45 s.

RNA Library Construction and Sequencing. Stranded mRNA-sequencing (seq) libraries were constructed with a SureSelect Strand Specific RNA Library Kit (Agilent Technologies) using polyA-selected mRNA extracted from two independent neuronal cultures containing latent POka VZV. Two hundred nanograms of total RNA was used as input. Samples were multiplexed and sequenced by NextSeq 550 using a 75-cycle V2 kit, producing 36.8 and 41.2 million 2 × 33-bp paired end reads per sample.

RNA-Seq Analysis. Quality control was performed by assessing various metrics (read duplication, transcript integrity scores, read distribution, and gene body coverage) using RSeQC (30). Paired-end reads were trimmed (Trim Galore, www.bioinformatics.babraham.ac.uk/projects/trim_galore/) and aligned against the *Homo sapiens* genome (HG19 assembly) using Tophat (31) to reduce the dataset. Unmapped read pairs were subsequently aligned against POka using Tophat, and fragments per kilobase of transcript per million mapped reads (FPKM) values were determined using cufflinks (32). Binary alignment/map (BAM) files were processed using SAMtools (33) and custom R scripts to produce maps of read coverage and depth across both strands of the VZV genome.

DNA Library Construction, Targeted Enrichment, and Sequencing. Sequence libraries were constructed and hybridized with custom-designed, VZV-specific, 120-mer RNA oligonucleotides as described previously (7), with the only modification being the use of 200 ng of starting DNA, as described in the SureSelect XT v1.6 protocol (Agilent Technologies). Sequencing libraries were multiplexed and sequenced on a single Illumina MiSeq run (500-bp V2 kit) yielding ~25 million paired-end reads.

Genome Assembly and Variant Calling. Following demultiplexing, each sequence dataset was profiled using FastQC (www.bioinformatics.babraham.ac.uk/projects/fastqc/) and parsed through QUASR (34) and Trim Galore for duplicate removal and read-trimming, respectively. Sequence reads were aligned against the VZV reference strain POka (AB097933) using Burrows–Wheeler alignment (35). Resulting alignments were processed using SAMtools (33) to generate pileup files for each sample. A consensus sequence for each dataset was called with the QUASR module pileupConsensus at an 80% frequency threshold (i.e., ambiguities were included if the variant frequency lay between 20% and 80%). Variant profiling for each dataset was performed using VarScan v2.2.11 (36) with the following parameters: base call quality ≥20, read depth ≥50, and independent reads supporting minor allele ≥2 per strand. In addition, variant calls showing directional strand bias ≥0.85 were excluded from further analyses. Before any analysis, the iterative repeat regions (R1, R2, R3, R4, and R5) and the terminal repeat region were masked.

Consensus Sequence and Variant Analyses. Consensus sequences were aligned using MAFFT (37), and resulting alignments were visually corrected using Mega v6 (38). Custom Perl scripts were used to profile differences between consensus sequences. For variant analyses, frequency plots were generated using custom R scripts.

Population Complexity Analysis Using Entropy. Entropy (*S*) is a measure of the diversity within a sample, with greater entropy indicating greater diversity. The formula for calculating the entropy of a position is:

$$\sum_{i-1}^{S}\left(\frac{Fi}{T}\right)-\log_b\left(\frac{Fi}{T}\right),$$

where *Fi* is the frequency of nucleotide *i*, *T* is the total number of nucleotides at the position, and base $b = 2$ for the logarithm. The entropy is calculated for each nucleotide with the entropy of each of the four nucleotides being summed to give the entropy of a position. Rare variants do not contribute much to the entropy because the log of their proportion will be very close to 0. The entropy of each position was calculated, and the entropy of each position was then summed to give the entropy of the sample.

Kolmogorov–Smirnov Test. The Kolmogorov–Smirnov (KS) test is used to determine if two datasets differ significantly without making any assumptions about the distribution of data. Here, two samples are plotted together in cumulative form, and each is scaled so their cumulative sums are 1.0. The KS statistic (D) reflects the greatest distance between the two. Critical values for the D statistic were determined by the number (N) of sites compared and was calculated as $1.36/(\sqrt{N})$ for $P = 0.05$. The null hypothesis (both sets of data are drawn from the same distribution) was rejected only if D exceeded the critical value and $P < 0.05$.

Results

VZV Infection of the Soma of Human Neurons Usually Induces a Productive Infection, Whereas Infection of Axons or Very-Low-Titer Infection of the Soma Results in Persistent Infection. Human NSCs were plated in the soma compartment of a microfluidic device (Fig. 1*A*, *Left*). Human neurons were obtained by differentiating NSCs, derived from hESCs (H9). Outgrowth of neurites was visible 3 d after differentiation of NSCs into neurons in the somal compartment and after 5–7 d in the axonal compartment. At 21–30 d after differentiation, axons were abundant in the axonal compartment and beta-III tubulin, a marker for neurons, was detected in >99% of the cells (Fig. 1*A*, *Right*). Less than 1% of the cells stained with Abs for astrocytes, and none of the cells stained with microglia or oligodendrocyte markers. Approximately 5% of the cells expressed peripherin and Brn3a, consistent with sensory neurons.

Neurons are highly permissive for infection with POka VZV, the parental virus of the live-attenuated VOka strain, when the cells are grown in vitro. Whereas neurons grown in typical cell cultures are infected with VZV at both the soma and axon simultaneously, neurons grown in microfluidic devices can be selectively

infected either at the somal compartment, where neuronal cell bodies, axons, and dendrites reside, or at the axonal compartment, where only distal axons and axon terminals reside. VZV POka cell-free virus (2×10^4 pfu/mL titrated on MRC-5 cells) was serially diluted (10-fold dilutions) from 0.5 μL (10 pfu on MRC-5 cells) to 0.0005 μL (0.01 pfu on MRC-5 cells), and neurons were infected at the soma. At 8 d postinfection (dpi), 0.5–0.005 μL of cell-free virus induced lytic infection and expressed abundant gE in neurons, whereas 0.0005 μL of cell-free virus did not result in gE expression (Fig. 1*B*). VZV DNA replication and gene expression were analyzed by qPCR using DNA and reverse transcriptase (RT)-qPCR using RNA, respectively (Fig. 1*C*). The quantity of VZV DNA in neurons increased at 8 d after somal infection with increasing amounts of virus from 0.0005 to 0.5 μL (Fig. 1*C*, *Left*; rows 1, 3, 5, and 7) or at 14 dpi with 0.0005–0.005 μL of virus (Fig. 1*C*, *Left*, rows 2 and 4), whereas the level plateaued at 14 dpi in neurons infected with 0.05 and 0.5 μL of virus (Fig. 1*C*, *Left*, rows 6 and 8). Genes from each of the kinetic classes of VZV, including ORF62 and ORF63 (immediate-early genes), ORF61 (putative immediate-early gene), ORF16 (putative early gene encoding a subunit of the viral DNA polymerase), and ORF42/45 (putative spliced late gene), were detected by RT-qPCR in neurons infected at the soma with 0.005–0.5 μL of cell-free virus (Fig. 1*C*, *Right*, rows 3–8). In contrast, although VZV DNA was present at 8 and 14 dpi with a very low amount (0.0005 μL) of cell-free virus, no viral gene expression was detected (Fig. 1*C*, *Right*, rows 1 and 2), suggesting that low-titer virus can infect neurons, but not result in detectable VZV gene expression or lytic replication. Additional experiments using 0.0005 μL of cell-free virus to infect the somal compartment showed persistence of viral DNA, but absence of detectable VZV gene expression even at 70 dpi. This result suggests that the cells may have been latently infected. However, we could not exclude the possibility that (*i*) cell-free virus persisted on the cell membrane without infecting the cell and/or (*ii*) free viral DNA present in the inoculum persists bound to the cell. The instability of cell-free virus produced in cell culture, the repeated washes after infection (including with low pH solution immediately after infection), and the long time between infection and assays for DNA and RNA (up to 70 d) all favor latent infection without gene expression.

To provide further evidence for latent infection of neurons in vitro, and to mimic what may occur in vivo, axons of neurons were infected with VZV POka in the microfluidic device using different doses of cell-free virus. The medium level was kept at least sevenfold higher in the somal compartment than in the axonal compartment of the device throughout the infection, including initial inoculation, washing steps, incubations, and changes of medium to induce a hydrostatic pressure gradient that prevents inoculum from diffusing from the axonal compartment to somal compartment (24–26), but does not prevent virus from being transported to the soma through axons. To our surprise, even when using the highest dose of VZV that could be applied to the axonal compartment (5 μL of cell-free virus + 5 μL of medium), neuronal cell bodies on the somal compartment did not show any expression of gE or cytopathic effect (CPE) at 8 dpi (Fig. 1*B*, *Right*), and no viral mRNA, including ORF63, was detected by RT-qPCR; however, VZV DNA was detectable by qPCR at 8 dpi and 14 dpi (Fig. 1*C*, rows 9 and 10, respectively). VZV DNA was detected in the soma at 2 hpi at the axonal compartment, and its persistence in the absence of detecting VZV mRNA was observed up to 70 dpi, suggesting that selective axonal infection of VZV in the microfluidic device results in persistent infection and may mimic latent infection that occurs in human ganglia. Axonal infection may be a relatively inefficient method to deliver VZV to the soma, relative to direct soma infection, and persistent infection might be favored over lytic infection simply by a very low quantity of VZV genomes in the soma.

Although no VZV RNA was detected by qPCR, deep sequencing using stranded RNA-seq of two independent POka-infected neuronal cultures after selective axonal infection for 14 dpi showed variable but low levels of transcription across all VZV ORFs (Fig. 1*D*). The pattern of VZV gene expression was consistent between both cultures and shared many characteristics with quiescent VZV obtained from neuronal cultures using a different system (21).

VZV Genome in Human Neurons Infected at the Axonal Compartment Is Maintained with Fused VZV Genomic Termini Consistent with an Episomal Configuration. In human trigeminal ganglia latently infected with VZV, the viral DNA persists with fused termini likely in a circular configuration (29). This observation is based on a ratio of terminal to internal DNA obtained by PCR reactions of 1 (1:1) for VZV DNA from latently infected ganglia compared with a ratio of 0.067 (1:15) for VZV DNA in virions. Cells undergoing lytic replication would be expected to have an intermediate ratio because they contain a mixture of virions and circular VZV DNA during rolling circular replication. If axonal infection of neurons with VZV in the microfluidic device mimics latency, the ratio of internal DNA to terminal DNA should be 1.

The ratio of fused terminal DNA (using primers T1 and T2) to internal DNA (using primers that detect ORF49) (Fig. 2*A*) was determined for the VZV_{Luc} BAC, which is a circular form of the genome, and set as 1 (Fig. 2*B*, lane 1). The ratio of fused terminal DNA to internal DNA for POka isolated from virions was 0.012 ± 0.001, indicating that it contains linear unit length genomes without fused termini with little or no intracellular circular, replicating VZV DNA (Fig. 2*B*, lane 2). In lytically infected neurons at 14 dpi, the ratio was 0.430 ± 0.0341 (Fig. 2*B*, lane 3). In neurons infected with POka by the axonal route, the ratio was 1.11 ± 0.257 at 14 dpi (Fig. 2*B*, lane 4), whereas in neurons infected with a very low MOI (10^{-7}) by the soma route, the ratio was 0.959 ± 0.0739 (Fig. 2*B*, lane 5). These data indicate that neurons persistently infected in vitro by the axonal route with VZV and without detectable expression of viral mRNA by RT-PCR harbor the genome with fused termini, likely in a circular or episomal genome, similar to what is seen in latently infected human ganglia.

Treatment of Persistently Infected Neurons with Ab to NGF Induces VZV Genome Replication, Expression of Viral mRNA, and Production of Infectious Virus. Latently infected cells have an intact viral genome that has the ability to reactivate and produce infectious virus. Therefore, we treated persistently infected neurons with several compounds known to reactivate other herpesviruses. These compounds included histone deacetylase (HDAC) inhibitors, such as butyric acid (8 mM), hexamethylene bisacetamide (10 mM), and valproic acid (5 mM), that have been shown to reactivate HSV and EBV (39) or a STAT3 inhibitor (10 mM S3I-201) or anti-NGF Ab that reactivates HSV (40–42). In neurons infected by the somal route with low-dose, cell-free POka VZV or at the axonal compartment in microfluidic devices with high-dose, cell-free virus, reactivation was not induced by treatment with HDAC or STAT3 inhibitors; however, treatment of neurons infected with POka by the axonal route with anti-NGF Ab (50 μg/mL) did induce VZV reactivation. At 14 d after axonal infection of neurons with 5 μL of POka cell-free VZV in a microfluidic device, there was no CPE and viral mRNA was not detected by RT-PCR; however, viral DNA was present. Seven days after adding anti-NGF Ab, some cells showed CPE in the microfluidic device. Cells were removed from the device, and one aliquot was used to isolate DNA and RNA. Viral DNA was increased after reactivation, and immediate-early, putative early, and putative late VZV genes were detected by qPCR in some (Fig. 3*A*, row 3), but not all (Fig. 3*A*, rows 1 and 5), somal compartments. The other aliquot of cells was treated with trypsin

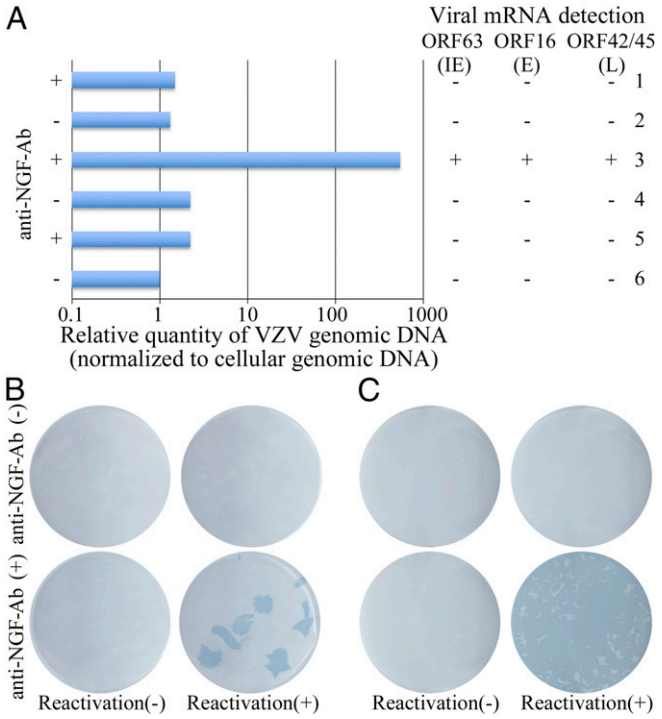

Fig. 3. Anti-NGF Ab induces VZV genome replication, mRNA expression, and production of infectious virus from neurons harboring persistent infection with fused VZV genomic termini. Neurons were infected with cell-free VZV at an MOI of 0.001 (titrated on MRC-5 cells) in the axonal compartment of microfluidic devices. At 14 dpi, anti-NGF sheep Ab (50 μg/mL), no Ab, or sheep IgG isotype control Ab (50 μg/mL) was added to the somal and axonal compartments. After 7 d, cells were removed from the device and divided into two equal fractions. (*A*) Relative quantity of VZV genomic DNA to cellular genomic DNA, as well as detection of VZV mRNAs, was determined as described in the legend for Fig. 1. (*B* and *C*) The other cell fraction was treated with trypsin and used to infect MRC-5 cells in duplicate. At 7 dpi, cells were fixed (*B*) or treated with trypsin and passaged onto uninfected MRC-5 cells and cultured for an additional 7 d (*C*). Cells were stained with VZV anti-gE Ab.

and used to infect MRC-5 cells. CPE and VZV gE expression was present in MRC-5 cells after 2–3 d, but only in the same compartments in which the neurons showed accumulation of VZV DNA and viral gene expression (Fig. 3*B*, *Lower Right* well). These results indicate that anti-NGF Ab was able to reactivate the viral genome, resulting in production of infectious virus. In the absence of anti-NGF Ab, no amplification of the viral genome was detected by qPCR, no detection of viral mRNA was found by RT-PCR (Fig. 3*A*, rows 2, 4, and 6), and no infectious virus or gE expression was present after transfer of neurons to MRC-5 cells (Fig. 3*B*, *Upper* wells). In four independent experiments, reactivation rates ranged from 17% to 33% with a mean of 27% after addition of anti-NGF Ab, whereas reactivation never occurred in the absence of the Ab or with addition of IgG isotype control Ab (Table 1). MRC-5 cells, which showed CPE after infection with the anti-NGF Ab–treated neurons, were passaged onto uninfected MRC-5 cells, and CPE and VZV gE was noted in the latter cells 7 dpi (Fig. 3*C*). In summary, because infectious VZV was produced from persistently infected neurons only after treatment with anti-NGF Ab, these infected neurons meet the criterion for latency.

VOka, Like POka, Can Establish Latency in Neurons in Vitro, but Is Impaired for Reactivation. VOka (3, 4) results in lower rates of zoster compared with WT virus in healthy and immunocompromised children (43–46). At present, it is unknown whether the vaccine virus is impaired for establishment of latency, reactivation, or both. Therefore, we compared the ability of POka and VOka to establish latency and reactivate in our in vitro latency model. Neurons were infected at the axonal compartment with an equal number of pfu (40 pfu) of cell-free POka and VOka. At 14 d after axonal infection, neurons infected with either virus showed no CPE and no viral mRNA was detected by RT-qPCR (Fig. 4*A*, *Right*); however, the VZV genomic DNA copy number in neurons was similar (Fig. 4*A*, *Left*). In neurons infected with VOka by the axonal route, the ratio of fused terminal DNA to internal DNA was 0.965 ± 0.135, indicating that VOka, like POka (Fig. 2*B*, lane 4), likely has a circular genome.

To compare the rate of reactivation of neurons infected with POka and VOka, anti-NGF Ab was added to the cells for 7 d, after which the neurons were removed and plated onto MRC-5 cells, and 7 d later, plaques were visualized and confirmed with anti-gE Ab (Fig. 4*B*). In four independent experiments ($n = 39$), the mean rate of reactivation was 23.1% for POka, compared with 5.1% for VOka (Table 2) ($P = 0.012$, two-tailed Student t test). These experiments imply that VOka can establish latency at a similar rate to POka, but that VOka is significantly impaired for reactivation compared with POka in vitro. Although it is possible that the reduced level of reactivation of VOka compared with POka was solely due to the slightly reduced DNA copy number of VOka in latently infected neurons, this possibility seems unlikely because the difference in the level of latent VOka and POka latent DNA was modest and not statistically significant ($P = 0.987$, two-tailed Student t test).

Deep sequencing using stranded RNA-seq of VOka-infected neuronal cultures after selective axonal infection for 14 dpi showed little or no transcription across VZV ORFs (Fig. 1*E*), which markedly differed from the pattern of transcription with POka-infected neurons (Fig. 1*D*). (Note that the scale of the peaks in the inner two circles for POka is 1,000-fold higher than the scale for VOka).

Comparative analysis of neuronal transcripts obtained from POka- and VOka-infected cultures revealed just eight differentially expressed genes, four of which are characterized (*CLEC4A*, *EGR1*, *CYR61*, and *SEMA3D*), whereas two remain uncharacterized and two are annotated as pseudogenes (Table S2).

VOka Undergoes a Loss in Heterogeneity During Reactivation in Vitro, but Not During Latency. Nine sequencing libraries were enriched for POka ($n = 4$) and VOka ($n = 5$) DNA, using SureSelect (7), that had sufficient reads to generate high-confidence genome assemblies where >99.9% of the genome was covered at read depths exceeding 50-fold (Table S3). VarScan (36) was used to report all sites at which a variant allele was present, either fixed or mixed with the reference allele. We compared variant allele frequencies between the input POka population and the latent POka population after 14 d (samples were from separate aliquots described in Fig. 4). We identified 42 sites with variant alleles, across the genome, 35 of which were present in both the input

Table 1. Frequency of reactivation of VZV POka in sectors from microfluidic devices

POka	No Ab			IgG control			Anti-NGF Ab		
Reactivation	−	+	%	−	+	%	−	+	%
Experiment 1	7	0	0		N.D.		5	2	28.6
Experiment 2	3	0	0		N.D.		2	1	33.3
Experiment 3		N.D.		6	0	0	5	1	16.7
Experiment 4		N.D.		10	0	0	7	3	30.0
Total	10	0	0	16	0	0	19	7	26.9

Numbers indicate number of sectors from microfluidic devices, with (+) or without (−) reactivation of VZV. N.D., not done.

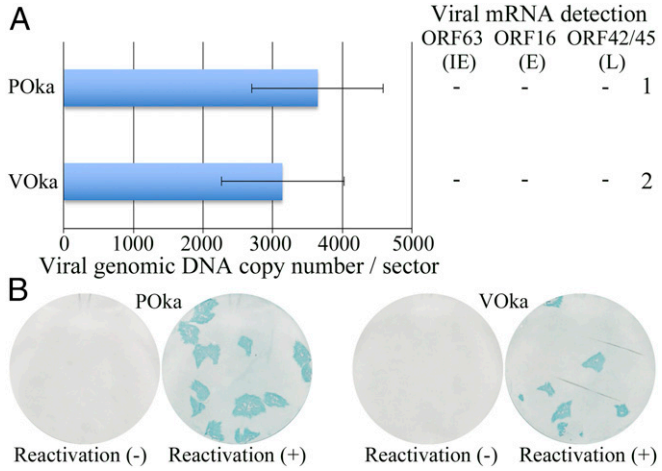

Fig. 4. VOka establishes latency at a similar rate to POka, but is impaired for reactivation in vitro. Neurons were infected with cell-free POka or VOka at an MOI of 0.001 (titrated on MRC-5 cells) in the axonal compartment of a microfluidic device. (*A*) At 14 dpi, DNA and RNA were extracted from four sectors each and RT-qPCR was performed. VZV genome DNA copy number and detection of VZV mRNAs were determined as described in the legend for Fig. 1. (*B*) At 14 dpi, reactivation was induced as described in the legend for Fig. 3. After another 7 d, neurons were plated onto MRC-5 cells and cultured for 7 d. Viral plaques were visualized as described in the legend for Fig. 3*C*.

and latent POka populations. Of these sites, 31 differed in allele frequency by less than 15% (mean = 6.5%) between input and latent POka. Seven new mutations [i.e., not present in the input POka (P1)], were present in latent POka, all at frequencies below 10% (Fig. S1). Variant alleles at nucleotides 58914 (ORF31, Q699R), 106262 (ORF62, R958G), and 109281 plus 110057 (both in the noncoding region between ORFs 62 and 63) increased by 17–42% in latent POka, whereas the variant at nucleotide 58914 (ORF31, R699) increased from 48% in the input pOka to 90% in the latent populations. There was no significant difference in the SNP frequencies between input and latent POka samples (KS test: D = 0.23, $P = 0.08$). Using entropy as a measure of population complexity, we observed only a very slight gain in heterogeneity between input ($S = 12.52$) and latent ($S = 13.58$–16.39) POka samples after 14 d (Fig. 5*A*).

Next, we compared variant allele frequencies between the input VOka population, the latent VOka population at 14 d after axonal infection, and the reactivated population 7 d after adding anti-NGF Ab (samples were from separate aliquots described in Fig. 4). We identified 195 polymorphic loci in the input genome, 143–160 in the latent samples, and 128–173 in the reactivated samples. Only a single site (100114, ORF58, K53N) was significantly changed between the input (36.69%) and the latent and reactivated samples (mean = 98.96%) (Fig. S2). Similarly, only a single variant allele (position 2493, noncoding, input = 6.63%) was consistently absent in the latent and reactivated samples. The viral population structures showed statistically significant changes between all three states (KS test: input vs. latent: D = 0.2826, $P < 0.01$; latent vs. reactivated: D = 0.3000, $P < 0.01$; input vs. reactivated: D = 0.3000, $P < 0.01$). However, the diversity and complexity (entropy), although similar for the input ($S = 71.79$) and latent ($S = 69.99$–87.19) VOka, were markedly higher than the entropy for reactivated virus ($S = 17.05$–26.2) (Fig. 5*B*). Thus, infection of neurons with VOka resulted in a loss in heterogeneity during reactivation in vitro, but not during latency.

Discussion

We have established an in vitro system for VZV latency and reactivation by selective infection of human neuronal axons with cell-free virus. We found that (*i*) VZV enters neurons without detectable viral gene expression by RT-qPCR or lytic replication, (*ii*) the VZV genome is maintained with fused termini indicative of an episomal configuration, and (*iii*) VZV can reactivate from neurons by the addition of anti-NGF Ab. Furthermore, comparison of infection of VOka and POka in our system showed that VOka can establish latency at a similar rate to POka, but VOka is impaired for reactivation. Neurons latently infected with VOka showed markedly reduced viral transcription based on deep sequencing using stranded RNA-seq compared with neurons latently infected with POka.

We found that axonal infection of neurons with cell-free virus resulted in a latent infection. In contrast, when we tested neurons by simultaneously infecting both the soma and axon using cell-free POka, we observed lytic infection leading to cell death, even at extremely low titers of virus (Fig. 1*B*). VZV infection of neurons has been postulated to occur either by retrograde axonal transport from cutaneous lesions or by hematogenous transfer of VZV to neurons in human ganglia during varicella. Evidence for infection from the bloodstream includes both animal models and clinical observations. The i.v. infection of VZV-infected human tonsil T cells can transfer VZV to neurons in human fetal ganglia xenografts in SCID-hu mice (47). In humans, multiple sensory ganglia (48) as well as enteric ganglia (1) are latently infected, consistent with viremic spread, because enteric ganglia do not project to the skin. There is also extensive clinical evidence for retrograde axonal transport of virus from infected epidermal or dermal cells to neurons in sensory ganglia. Herpes zoster occurs most frequently on the face and upper thorax, which is the area most severely affected by varicella (48, 49). Herpes zoster associated with varicella vaccine is most common at the site of the vaccine inoculation (43), and about 50% of zoster cases associated with vaccination are due to WT virus (50). Also, VZV has previously been shown to enter neurons in vitro from nerve endings by cell-to-cell contact with infected cells or cell-free virus followed by transaxonal transport to the soma (16, 17, 21).

Although we were able to obtain latent infection of neurons using axonal infection in a microfluidic device, other studies reported a lytic infection using this route (16, 17). These studies differed from ours in that they used cell-associated virus, whereas we used cell-free virus. Markus et al. (21) described two in vitro models of latency and reactivation of VZV in hESC-derived neurons. In the first model, human neurons were infected at the somal site (in the absence of a microfluidic device) using low-dose, cell-free, POka-based GFP recombinant virus in the presence of acyclovir. A nonproductive, persistent infection was observed in which viral DNA and transcripts for IE63 and ORF31 (a putative late gene) were detected by qPCR, and transcripts from all genomic regions were detected by RNA-seq analysis. Reactivation could be induced by removal of acyclovir and replacing the medium with new medium lacking three neurotrophin growth factors (NGF, BDNF, and NT3) that had been present or by adding a PI3K inhibitor or sodium butyrate.

Table 2. Frequency of reactivation of VZV POka or VOka in sectors from microfluidic devices

POka vs. VOka	POka			VOka		
Reactivation	–	+	%	–	+	%
Experiment 1	8	1	11.1	9	0	0
Experiment 2	7	3	30.0	9	1	10.0
Experiment 3	8	2	20.0	9	1	10.0
Experiment 4	7	3	30.0	10	0	0
Total	30	9	23.1	37	2	5.1

Numbers indicate number of sectors from microfluidic devices, with (+) or without (–) reactivation of VZV.

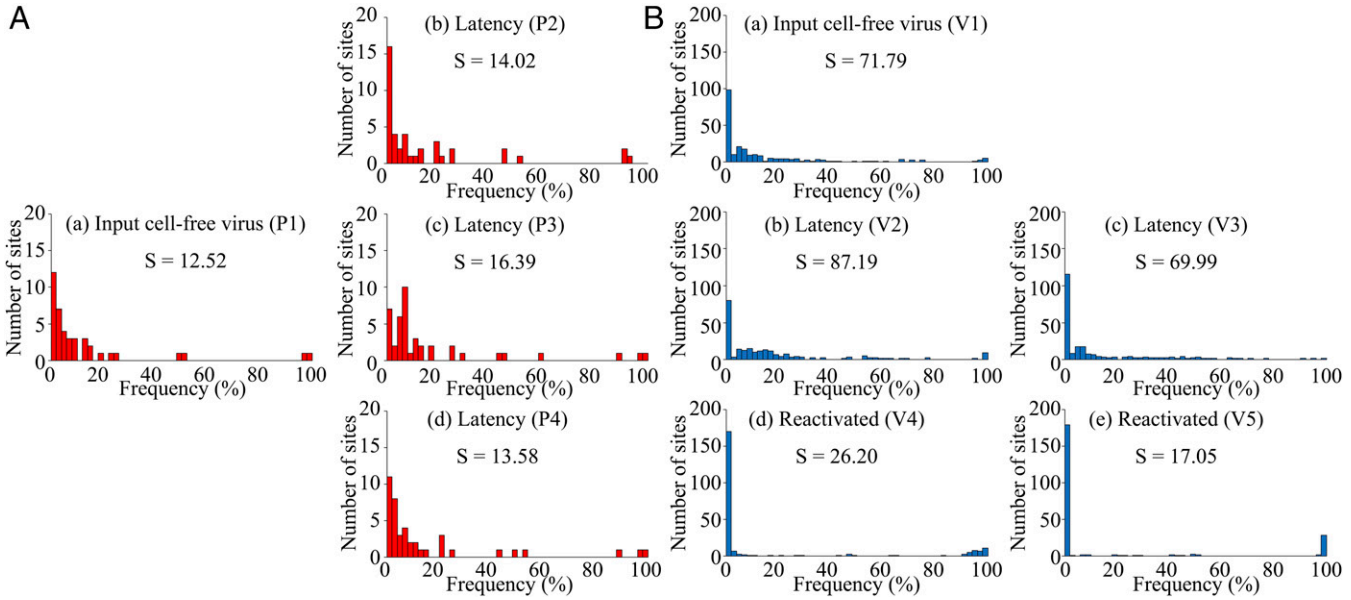

Fig. 5. VOka maintains its heterogeneity during latency, but not during reactivation in vitro. Whole-genome sequencing analyses were performed for POka (*A*) and VOka (*B*), and their complexity was determined by analyzing the number of sites undergoing nucleotide changes and calculating the entropy (*S*). (*A*) POka DNA was extracted from input cell-free virus (*a*) and from different aliquots of latent viral DNA (*b*–*d*) at 14 dpi (Fig. 4). (*B*) VOka DNA was extracted from input cell-free virus (*a*), different aliquots of latent viral DNA at 14 dpi (*b* and *c*), and reactivated (*d* and *e*) viral DNA at 7 d (before adding to MRC-5 cells, as shown in Fig. 4). Frequency histograms denote the frequency distribution of variant alleles. Data are binned at 2% intervals along the *x* axis, and the numbers of variant sites in each bin are shown on the *y* axis. Entropy, analogous to population diversity, was determined for each individual sample.

In the second model, neurons were infected with VZVORF66GFP recombinant virus in the axonal compartment of a microfluidic chamber in the absence of acyclovir. Both VZV DNA and transcripts for IE63 and ORF31 were detected 2 wk after infection by PCR, but RNA-seq analysis was not performed; treatment of the cells with a PI3K inhibitor resulted in increased VZV DNA and RNA expression, and, after reducing the temperature to 34 °C, GFP expression was detected in a few cells. Our system differs from the second model (21), which also used a microfluidic device, in several respects. First, we used POka, a nonrecombinant virus, which should be very similar to virus isolated from patients. Second, we could not detect VZV mRNAs during latency, including immediate-early (ORF61, ORF62, ORF63), putative early (ORF16), and putative late (ORF42/45) genes, by RT-qPCR using an assay that detects less than 10 copies of mRNA per reaction. Third, we demonstrated that virus could be passaged to a different cell type. Fourth, our experiments were performed at 37 °C, and we did not need to reduce the temperature to 34 °C to observe full evidence of reactivation. Fifth, we induced reactivation by adding anti-NGF Ab; in fact, we could not reactivate virus using a PI3K inhibitor.

We found that axonal infection with cell-free virus resulted in latent infection without detectable viral gene expression by RT-qPCR. VZV latency has been defined using human cadaveric ganglia, because of a lack of in vitro or in vivo models that reproduce both latency and reactivation. Although multiple viral proteins have been detected by immunohistochemistry in human cadaveric ganglia (reviewed in ref. 51), recent studies showed that anti-VZV mouse mAbs obtained from ascites and anti-VZV rabbit polyclonal Abs contain Abs to human blood group A1-associated antigens (13, 14), which casts doubt on the presence of VZV proteins during latency in human ganglia in some prior reports (2). Initial studies of VZV transcription in human ganglia used tissues obtained at various times postmortem, and utilizing a variety of techniques, multiple transcripts were detected (reviewed in ref. 51). More recent studies suggest that transcription of VZV during latency in human ganglia may be more limited. When human ganglia were obtained less than 9 h postmortem, no VZV RNAs could be detected by multiplex RT-PCR, and only ORF63 mRNA could be detected by RT-qPCR (15). In contrast, multiple VZV mRNAs were detected when ganglia were obtained 9 h or more postmortem, and higher levels of ORF63 mRNA were also seen later postmortem. These results suggest that detection of multiple VZV mRNAs in human cadaveric ganglia may reflect reactivation postmortem rather than true latent infection. Studies of ganglia obtained from the intestines of children soon after surgical excision, who had a history of varicella, showed ORF63 mRNA in 83% of specimens followed by ORF4 in 67% (1). At present, it remains controversial as to which VZV proteins and transcripts are expressed during VZV latency in vivo (reviewed in 51). VZV latency may be similar to HSV, with most latently infected cells expressing no viral mRNAs or proteins (51). Thus, the inability to detect VZV transcripts by RT-qPCR in our in vitro model of VZV latency may reflect the state of latency in human ganglia during life. However, we found that RNA-seq analysis detected transcripts for all annotated genes during latency in vitro. Whether these low-level transcripts are functional or not is unclear. We are not aware of any published studies using RNA-seq and VZV or HSV latently infected human ganglia, so it is unclear if low levels of viral transcripts are present in these tissues. However, RNA-seq analysis of latent EBV Burkitt lymphoma cells shows transcription across the viral genome (52).

The in vitro latency system that we describe differs from latently infected sensory ganglia in several aspects. More than 99% of the cells we infected expressed neuronal markers; therefore, our system contains few, if any, of the other cell types present in sensory ganglia, such as satellite cells, fibroblasts, and immune cells (e.g., macrophages, lymphocytes). Thus, many cell–cell interactions and soluble factors secreted by nonneuronal cells that are present in sensory ganglia are absent in our system. It is possible that the absence of detectable VZV gene expression by RT-PCR in our system may be due to the lack of nonneuronal cells that could influence viral gene expression in neurons. In addition, only

~5% of the neurons in our system expressed markers of sensory neurons, indicating that there was a heterogeneous population of neurons present. Thus, the composition of neurons in our system differs from the composition of neurons in sensory ganglia.

We found that the VZV genome maintained in human neurons had fused VZV genomic termini consistent with an episomal configuration. A prior study with latently infected human ganglia showed that the viral genome had fused termini likely from a circular or concatemeric configuration (29). Herpesvirus genomes are present in a unit length linear configuration within nucleocapsids and quickly circularize after entering the nucleus (51). Long head-to-tail concatemers of viral DNA are produced by rolling circle DNA replication by viral DNA replication proteins (51). Our in vitro model of VZV latency in the absence of gene expression by RT-qPCR suggests that the VZV genome exists as a circular configuration rather than as concatemers.

We showed that treatment of latently infected neurons with neutralizing Ab to NGF induced VZV genome replication and expression of viral mRNA with production of infectious virus. An in vitro model of HSV latency was developed in which HSV-1–infected neurons from neonatal rat cervical ganglia are incubated with NGF; acyclovir is required to maintain latency in this system (40). Treatment of the virus-infected neurons with anti-NGF Ab resulted in HSV-1 reactivation. The molecular mechanisms for reactivation of VZV resulting in herpes zoster are less clear, but trauma (53) and neurosurgical procedures (54, 55) have been associated with zoster. Retrograde NGF signaling from the axon to the soma is critical for maintenance and survival of sensory and sympathetic neurons (56, 57). Therefore, axonal injury by trauma or neurosurgical procedures might reduce NGF signaling not only by interrupting retrograde transport but also by altering mRNA transcription and translation (58). The ability of VZV to reactivate by inhibiting NGF in our in vitro system may mimic what occurs during axonal injury in vivo.

VOka establishes latency after vaccination, and the virus can reactivate (1, 59). The rate of herpes zoster is lower after vaccination with VOka compared with natural infection (43–46), implying that the vaccine virus is attenuated for latency and/or reactivation. We found that VOka can establish latency at a similar rate as POka, but is significantly impaired for reactivation from latency in vitro. However, there was markedly reduced viral transcription during latency in neurons infected with VOka compared with POka. These results suggest that extensive viral transcription was not required to maintain latency. Deep sequencing showed that VOka undergoes a loss in heterogeneity during reactivation in vitro, but not during latency. This loss in heterogeneity could be due to a selection for specific viral genotypes or a stochastic process related to the low numbers of sequences recovered during reactivation. The latter hypothesis may be more likely, because a study of rashes in persons receiving Oka vaccine virus showed that genotypes in rashes after vaccination or due to reactivation from latency were similar (7).

The in vitro model of VZV latency and reactivation we report might be used to study the mechanism of VZV latency and reactivation and to screen for inhibitors of reactivation or molecules that might reduce the number of latently infected neurons. Furthermore, this system may also be used to study candidate viral vaccines for their ability to establish latency and reactivate.

ACKNOWLEDGMENTS. This work was supported by the intramural research program of the National Institute of Allergy and Infectious Diseases. T.S. was supported by the Japan Herpesvirus Infections Forum. D.P.D. is supported by a New Investigator Award from the Medical Research Foundation [UK Medical Research Council (MRC)]. J.B. was partially funded by the UCL/UCLH Biomedical Research Centre (BRC). A.V. received funding from the Maryland Stem Cell Research Fund. We acknowledge support from the MRC and BRC for the UCL/UCLH Pathogen Sequencing Pipeline.

1. Gershon AA, et al. (2012) Latency of varicella zoster virus in dorsal root, cranial, and enteric ganglia in vaccinated children. *Trans Am Clin Climatol Assoc* 123:17–33; discussion 33–35.
2. Arvin AM, Gilden D (2013) Varicella-zoster virus. *Fields Virology*, eds Knipe DM, Howley PM (Wolters Kluwer Health, Philadelphia), 6th Ed, pp 2015–2057.
3. Takahashi M, Otsuka T, Okuno Y, Asano Y, Yazaki T (1974) Live vaccine used to prevent the spread of varicella in children in hospital. *Lancet* 2(7892):1288–1290.
4. Takahashi M (1984) Development and characterization of a live varicella vaccine (Oka strain). *Biken J* 27(2-3):31–36.
5. Gomi Y, Imagawa T, Takahashi M, Yamanishi K (2000) Oka varicella vaccine is distinguishable from its parental virus in DNA sequence of open reading frame 62 and its transactivation activity. *J Med Virol* 61(4):497–503.
6. Gomi Y, et al. (2002) Comparison of the complete DNA sequences of the Oka varicella vaccine and its parental virus. *J Virol* 76(22):11447–11459.
7. Depledge DP, et al. (2014) Deep sequencing of viral genomes provides insight into the evolution and pathogenesis of varicella zoster virus and its vaccine in humans. *Mol Biol Evol* 31(2):397–409.
8. Zerboni L, et al. (2005) Analysis of varicella zoster virus attenuation by evaluation of chimeric parent Oka/vaccine Oka recombinant viruses in skin xenografts in the SCIDhu mouse model. *Virology* 332(1):337–346.
9. Quinlivan M, Breuer J (2014) Clinical and molecular aspects of the live attenuated Oka varicella vaccine. *Rev Med Virol* 24(4):254–273.
10. Cohen JI (2010) Rodent models of varicella-zoster virus neurotropism. *Curr Top Microbiol Immunol* 342:277–289.
11. Mahalingam R, Messaoudi I, Gilden D (2010) Simian varicella virus pathogenesis. *Curr Top Microbiol Immunol* 342:309–321.
12. Azarkh Y, Gilden D, Cohrs RJ (2010) Molecular characterization of varicella zoster virus in latently infected human ganglia: Physical state and abundance of VZV DNA, Quantitation of viral transcripts and detection of VZV-specific proteins. *Curr Top Microbiol Immunol* 342:229–241.
13. Zerboni L, et al. (2012) Apparent expression of varicella-zoster virus proteins in latency resulting from reactivity of murine and rabbit antibodies with human blood group a determinants in sensory neurons. *J Virol* 86(1):578–583.
14. Ouwendijk WJD, et al. (2012) Immunohistochemical detection of intra-neuronal VZV proteins in snap-frozen human ganglia is confounded by antibodies directed against blood group A1-associated antigens. *J Neurovirol* 18(3):172–180.
15. Ouwendijk WJD, et al. (2012) Restricted varicella-zoster virus transcription in human trigeminal ganglia obtained soon after death. *J Virol* 86(18):10203–10206.
16. Markus A, et al. (2011) Varicella-zoster virus (VZV) infection of neurons derived from human embryonic stem cells: Direct demonstration of axonal infection, transport of VZV, and productive neuronal infection. *J Virol* 85(13):6220–6233.
17. Grigoryan S, et al. (2012) Retrograde axonal transport of VZV: Kinetic studies in hESC-derived neurons. *J Neurovirol* 18(6):462–470.
18. Jones JO, Arvin AM (2003) Microarray analysis of host cell gene transcription in response to varicella-zoster virus infection of human T cells and fibroblasts in vitro and SCIDhu skin xenografts in vivo. *J Virol* 77(2):1268–1280.
19. Jones M, et al. (2014) RNA-seq analysis of host and viral gene expression highlights interaction between varicella zoster virus and keratinocyte differentiation. *PLoS Pathog* 10(1):e1003896.
20. Markus A, Waldman Ben-Asher H, Kinchington PR, Goldstein RS (2014) Cellular transcriptome analysis reveals differential expression of pro- and antiapoptosis genes by varicella-zoster virus-infected neurons and fibroblasts. *J Virol* 88(13):7674–7677.
21. Markus A, Lebenthal-Loinger I, Yang IH, Kinchington PR, Goldstein RS (2015) An in vitro model of latency and reactivation of varicella zoster virus in human stem cell-derived neurons. *PLoS Pathog* 11(6):e1004885.
22. Sadaoka T, et al. (2014) Varicella-zoster virus ORF49 functions in the efficient production of progeny virus through its interaction with essential tegument protein ORF44. *J Virol* 88(1):188–201.
23. Tegenge MA, et al. (2014) Curcumin protects axons from degeneration in the setting of local neuroinflammation. *Exp Neurol* 253:102–110.
24. Hosmane S, Yang IH, Ruffin A, Thakor N, Venkatesan A (2010) Circular compartmentalized microfluidic platform: Study of axon-glia interactions. *Lab Chip* 10(6): 741–747.
25. Hosmane S, et al. (2012) Toll/interleukin-1 receptor domain-containing adapter inducing interferon-β mediates microglial phagocytosis of degenerating axons. *J Neurosci* 32(22): 7745–7757.
26. Rajbhandari L, et al. (2014) Toll-like receptor 4 deficiency impairs microglial phagocytosis of degenerating axons. *Glia* 62(12):1982–1991.
27. Li Q, et al. (2010) Insulin degrading enzyme induces a conformational change in varicella-zoster virus gE, and enhances virus infectivity and stability. *PLoS One* 5(6): e11327.
28. Zhang Z, et al. (2007) Genetic analysis of varicella-zoster virus ORF0 to ORF4 by use of a novel luciferase bacterial artificial chromosome system. *J Virol* 81(17):9024–9033.
29. Clarke P, Beer T, Cohrs R, Gilden DH (1995) Configuration of latent varicella-zoster virus DNA. *J Virol* 69(12):8151–8154.
30. Wang L, Wang S, Li W (2012) RSeQC: Quality control of RNA-seq experiments. *Bioinformatics* 28(16):2184–2185.
31. Trapnell C, Pachter L, Salzberg SL (2009) TopHat: Discovering splice junctions with RNA-Seq. *Bioinformatics* 25(9):1105–1111.
32. Trapnell C, et al. (2010) Transcript assembly and quantification by RNA-Seq reveals unannotated transcripts and isoform switching during cell differentiation. *Nat Biotechnol* 28(5):511–515.

33. Li H, et al.; 1000 Genome Project Data Processing Subgroup (2009) The Sequence Alignment/Map format and SAMtools. *Bioinformatics* 25(16):2078–2079.
34. Watson SJ, et al. (2013) Viral population analysis and minority-variant detection using short read next-generation sequencing. *Philos Trans R Soc Lond B Biol Sci* 368(1614): 20120205.
35. Li H, Durbin R (2009) Fast and accurate short read alignment with Burrows-Wheeler transform. *Bioinformatics* 25(14):1754–1760.
36. Koboldt DC, et al. (2012) VarScan 2: Somatic mutation and copy number alteration discovery in cancer by exome sequencing. *Genome Res* 22(3):568–576.
37. Katoh K, Standley DM (2013) MAFFT multiple sequence alignment software version 7: Improvements in performance and usability. *Mol Biol Evol* 30(4):772–780.
38. Tamura K, Stecher G, Peterson D, Filipski A, Kumar S (2013) MEGA6: Molecular Evolutionary Genetics Analysis version 6.0. *Mol Biol Evol* 30(12):2725–2729.
39. Hafezi W, et al. (2012) Entry of herpes simplex virus type 1 (HSV-1) into the distal axons of trigeminal neurons favors the onset of nonproductive, silent infection. *PLoS Pathog* 8(5):e1002679.
40. Wilcox CL, Johnson EM, Jr (1987) Nerve growth factor deprivation results in the reactivation of latent herpes simplex virus in vitro. *J Virol* 61(7):2311–2315.
41. Du T, Zhou G, Roizman B (2013) Modulation of reactivation of latent herpes simplex virus 1 in ganglionic organ cultures by p300/CBP and STAT3. *Proc Natl Acad Sci USA* 110(28):E2621–E2628.
42. Camarena V, et al. (2010) Nature and duration of growth factor signaling through receptor tyrosine kinases regulates HSV-1 latency in neurons. *Cell Host Microbe* 8(4): 320–330.
43. Hardy I, Gershon AA, Steinberg SP, LaRussa P; Varicella Vaccine Collaborative Study Group (1991) The incidence of zoster after immunization with live attenuated varicella vaccine. A study in children with leukemia. *N Engl J Med* 325(22):1545–1550.
44. Baxter R, et al. (2013) Long-term effectiveness of varicella vaccine: A 14-Year, prospective cohort study. *Pediatrics* 131(5):e1389–e1396.
45. Son M, et al. (2010) Effectiveness of varicella vaccine in children infected with HIV. *J Infect Dis* 201(12):1806–1810.
46. Tseng HF, Smith N, Marcy SM, Sy LS, Jacobsen SJ (2009) Incidence of herpes zoster among children vaccinated with varicella vaccine in a prepaid health care plan in the United States, 2002-2008. *Pediatr Infect Dis J* 28(12):1069–1072.
47. Zerboni L, Ku C-C, Jones CD, Zehnder JL, Arvin AM (2005) Varicella-zoster virus infection of human dorsal root ganglia in vivo. *Proc Natl Acad Sci USA* 102(18): 6490–6495.
48. Mahalingam R, et al. (1990) Latent varicella-zoster viral DNA in human trigeminal and thoracic ganglia. *N Engl J Med* 323(10):627–631.
49. Hope-Simpson RE (1965) The nature of herpes zoster: A long-term study and a new hypothesis. *Proc R Soc Med* 58:9–20.
50. Weinmann S, et al. (2013) Incidence and clinical characteristics of herpes zoster among children in the varicella vaccine era, 2005-2009. *J Infect Dis* 208(11):1859–1868.
51. Kennedy PGE, Rovnak J, Badani H, Cohrs RJ (2015) A comparison of herpes simplex virus type 1 and varicella-zoster virus latency and reactivation. *J Gen Virol* 96(Pt 7): 1581–1602.
52. Lin Z, et al. (2010) Quantitative and qualitative RNA-Seq-based evaluation of Epstein-Barr virus transcription in type I latency Burkitt's lymphoma cells. *J Virol* 84(24): 13053–13058.
53. Zhang JX, Joesoef RM, Bialek S, Wang C, Harpaz R (2013) Association of physical trauma with risk of herpes zoster among Medicare beneficiaries in the United States. *J Infect Dis* 207(6):1007–1011.
54. Godfrey EK, Brown C, Stambough JL (2006) Herpes zoster–varicella complicating anterior thoracic surgery: 2 case reports. *J Spinal Disord Tech* 19(4):299–301.
55. Simms HN, Dunn LT (2006) Herpes zoster of the trigeminal nerve following microvascular decompression. *Br J Neurosurg* 20(6):423–426.
56. Freeman RS, et al. (2004) NGF deprivation-induced gene expression: After ten years, where do we stand? *Prog Brain Res* 146:111–126.
57. Zweifel LS, Kuruvilla R, Ginty DD (2005) Functions and mechanisms of retrograde neurotrophin signalling. *Nat Rev Neurosci* 6(8):615–625.
58. Jung H, Yoon BC, Holt CE (2012) Axonal mRNA localization and local protein synthesis in nervous system assembly, maintenance and repair. *Nat Rev Neurosci* 13(5):308–324.
59. Gershon AA, Gershon MD (2013) Pathogenesis and current approaches to control of varicella-zoster virus infections. *Clin Microbiol Rev* 26(4):728–743.